

Topological Classification of One-Dimensional Chiral Symmetric Interfaces

Harry MullineauxSanders and Bernd Braunecker
*SUPA, School of Physics and Astronomy, University of St. Andrews,
North Haugh, St. Andrews KY16 9SS, United Kingdom*
(Dated: July 2, 2024)

We address the topological classification of one-dimensional chiral symmetric interfaces embedded into a two-dimensional substrate. A proof of the validity of a topological classification based on the Green's function by explicit evaluation of the topological invariant is presented. Further, we show that due to entanglement between the in-gap modes and the substrate, the full physics of the substrate that is contained in the Green's function is required. This is done by considering a classification scheme derived from the reduced ground state projector, for which we show that an uncritical handling produces erroneous changes in the topological index due to entanglement driven gap closures. We illustrate our results by applying them to a tight-binding model of a spiral magnetic interface in a s-wave superconductor.

The realisation of topological quantum states has been a major aim of condensed matter physics for a number of years. Most prominent is the task of obtaining robust Majorana modes at the edge of materials or in vortex cores [1–3], as they also would provide the first steps towards topological quantum computation [4, 5]. In the absence of topological properties in a bulk material [6], artificially created topological superconductors in superconductor-semiconductor structures [7] or magnetic-superconductor interfaces [8] have emerged as promising candidates for the creation of tunable topological states. The latter, specifically chains of magnetic impurities on standard s-wave superconductors, have been a source of great interest in recent years.

Magnetic impurities locally break apart Cooper pairs, lowering the superconducting gap [9, 10] and creating bound Yu-Shiba-Rusinov electronic states [11–13]. Chains of impurities, such as shown in Fig. 1, then create in-gap bands [12] which can be taken through a topological phase transition by tuning the magnetic scattering strength and the magnetic alignment. The topological properties of these kinds of magnetic interfaces have been determined by exact diagonalisation of tight-

binding models [8, 9, 14–16], by first principles numerical calculation of the Green's function [17–19], by analytic determination of the Green's function with a Debye frequency cut off [20], by effective tight-binding hybridisation of the impurity states, [21–26], and by modelling a one-dimensional (1D) magnetic wire placed in proximity to a superconductor which can be integrated out [27, 28]. In the case of densely packed impurity chains, the effect of the dimensionally embedded nature of the interface on the band structure and topological properties has been derived from an exact determination of the Green's function [29–33]. There has also been significant experimental effort in fabricating and studying these interfaces, some of which have shown signs of topological physics [34–41].

As the topological properties are due to the 1D interface, in many approaches topological invariants are derived from an effective 1D Hamiltonian. However it was shown in Ref. [31], that any topological classification based on integrating the transverse spatial degrees of freedom out of the Hamiltonian is only valid in the specific limit of tightly confined impurity bound modes, which typically is not realised in experiment [36]. The central problem with such a tracing over the transverse spatial dimension is that essential information is lost or falsified if the in-gap mode has entanglement between its inter-unit-cell and spatial degrees of freedom. This is at the risk that topological properties are not correctly reproduced [31]. A further complication from the large spatial extent of the in-gap states is that a simple modelling based on the hybridisation of single impurity modes is insufficient to capture essential features such as gap closures around the Fermi momentum or dimensional renormalisation of the scattering strength at phase transitions [30]. In the absence of an effective 1D Hamiltonian from which an effective ground state projector can be derived, standard topological classification methods are unavailable. Therefore topological properties must be derived from an (ideally analytically and experimentally) available quantity. Such classification schemes have been proposed but only with circumstantial conjecture of their validity.

In this paper, we provide a general proof of valid-

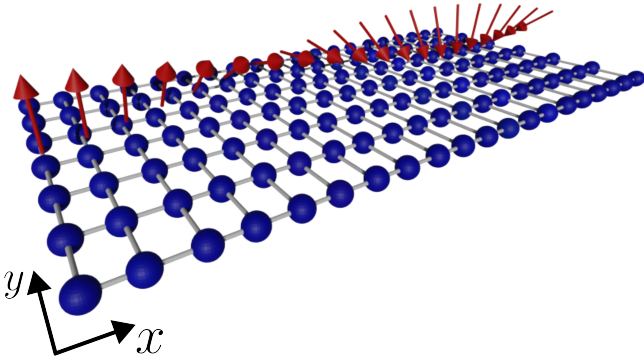


FIG. 1. Sketch of a generic spiral magnetic interface model: A square lattice tight-binding model of a s-wave superconducting substrate with a chain of spiralling magnetic impurities along the x direction.

ity of an approach based on local Green's functions [31, 32], and extend its validity to any chiral symmetry class. To illustrate the scheme's applicability we use it to obtain the full topological phase diagram of a tight binding model of a magnetic interface embedded in a superconductor, by exactly solving for the Green's function. To demonstrate further that this method is resilient against the aforementioned reduction of spatial degrees of freedom, we compare it with the reduced ground state projector approach of Ref. [42]. We demonstrate that in the parameter regions of most interest, the two-dimensional (2D) extension of the in-gap modes is significant enough that the latter approach requires careful handling to avoid artefacts of the truncation.

Topological Hamiltonian – We consider topological invariants based on an effective topological Hamiltonian obtained from the local Green's function. This has been proposed before [31, 32] and observed to be consistent with the correct topological classification but without the general proof of validity which we shall provide.

To this end we consider a gapped 2D translationally invariant substrate with Hamiltonian $\mathcal{H}_0(k_x, k_y)$, for momenta k_x, k_y , and energies chosen such that the gap is centred about energy $\omega = 0$. A scattering interface is introduced as a strip along the x direction that is bounded in the y direction. For simplicity, we take the interface to be only at $y = 0$ (such as in Fig. 1), however our results generalise straightforwardly to wider interfaces. In such a case case, the y dimension is partitioned into segments of the width of the interface, and the y coordinate then labels each segment whereas the spatial dependence within a segment is taken as an internal degree of freedom. Assuming translational invariance along the x direction, we define the projector onto the interface as $P_{y=0}$ and its scattering Hamiltonian $\mathcal{H}_V(k_x) = H_V(k_x) \otimes P_{y=0}$ where H_V acts on the remaining degrees of freedom.

We denote by $g(\omega, k_x, y)$ the retarded Green's function at energy ω of $\mathcal{H}_0(k_x, k_y)$ after the partial Fourier transform $k_y \rightarrow y$. Then the total retarded Green's function of $\mathcal{H} = \mathcal{H}_0 + \mathcal{H}_V$ with broken translational invariance in the y direction is given by the Dyson equation [43]

$$G(\omega, k_x, y, y') = g(\omega, k_x, y - y') + g(\omega, k_x, y)T(\omega, k_x)g(\omega, k_x, -y'), \quad (1)$$

where the effect of H_V is contained in the T -matrix

$$T(\omega, k_x) = [H_V^{-1} - g(\omega, k_x, 0)]^{-1}. \quad (2)$$

If bound states appear at the interface, their energies are given by the poles of T as a function of ω , and the corresponding residues provide information about their wavefunctions. Consequently T , and thus G , are expected to contain all topological information too, and it was proposed in Refs. [31, 32] that

$$H^{top}(k_x, y) = -[G(\omega = 0, k_x, y, y)]^{-1} \quad (3)$$

forms a suitable topological Hamiltonian for the topological classification. Similar Hamiltonians have been used

to study interacting topological materials [44, 45]. When $y = 0$, the chiral invariant of this topological Hamiltonian for a spiral magnetic superconductor interface has been shown to match the Pfaffian invariant calculated from a tight-binding model [32] and the presence of Majorana edge modes [31]. For $y \neq 0$, zeros of the Green's function create fictitious phase boundaries which perfectly cancel the true phase boundaries as $|y| \rightarrow \infty$ so $H^{top}(|y| \rightarrow \infty)$ is always trivial [31].

We shall now provide a proof of the general applicability of H^{top} for the topological classification, and we shall show that the topological invariant calculated from H^{top} for a system with chiral symmetry separates into contributions given by an invariant of the substrate and of the in-gap bands separately. To demonstrate the applicability it is sufficient to demonstrate that the topological Hamiltonian possesses the same global symmetries as the full 2D Hamiltonian. Let $\mathcal{H}(k_x)$ be the full Hamiltonian at a fixed k_x and consider it as a matrix that acts on all other degrees of freedom including y . The Green's function is defined by $G(\omega, k_x) = [\omega \mathbb{1} - \mathcal{H}(k_x)]^{-1}$ and as the Hamiltonian is gapped, $G(\omega = 0, k_x) = -[\mathcal{H}(k_x)]^{-1}$ is non-singular. If $\tilde{\Lambda}$ is a symmetry operator such that $\tilde{\Lambda}\mathcal{H}(k_x)\tilde{\Lambda} = \pm\mathcal{H}(\pm k_x)$ for a given combination of \pm signs, then $\tilde{\Lambda}G(0, k_x)\tilde{\Lambda} = \pm G(0, \pm k_x)$ holds as well [46]. If $\tilde{\Lambda}$ is global such that $\tilde{\Lambda} = \Lambda \otimes \mathbb{1}_y$ where $\mathbb{1}_y$ is the identity for the y coordinate and Λ acts on the remaining degrees of freedom [42], then it commutes with the projection onto y and it follows that

$$\Lambda^{-1}G(\omega = 0, k_x, y, y)\Lambda = \pm G(\omega = 0, \pm k_x, y, y). \quad (4)$$

Therefore the local Green's function, and consequently $H^{top}(k_x, y)$ satisfy all the global symmetries of the full Hamiltonian. Further, as proven in Appendix A, since the interface region is bounded, the following theorem is true:

$$\begin{aligned} \text{The Hamiltonian } \mathcal{H} = \mathcal{H}_0 + \mathcal{H}_V \text{ possesses} & \quad (5) \\ \text{a global symmetry } \Lambda \otimes \mathbb{1}_y & \end{aligned}$$

\Leftrightarrow

Λ is a symmetry of $g(0, k_x, y)$ and H_V individually.

It follows then from Eq. (2) that the T -matrix also possesses the same symmetry. This means in any symmetry class, we can define a topological invariant of the topological Hamiltonian, the substrate Green's function, the T -matrix and the scattering Hamiltonian separately.

We now specialise our discussion to chiral 1D symmetry classes which is relevant to magnetic impurity-superconductor interfaces [31, 32, 47]. In these classes, the Hamiltonian, $\mathcal{H}(k_x)$, has a unitary Hermitian symmetry \mathcal{C} such that $\mathcal{C}\mathcal{H}(k_x)\mathcal{C} = -\mathcal{H}(k_x)$. In this case the appropriate topological invariant is the winding number, W , calculated by writing the topological Hamiltonian in the eigenbasis of the chiral operator [48]

$$H^{top}(k_x, y) = \begin{pmatrix} 0 & h(k_x, y) \\ h^\dagger(k_x, y) & 0 \end{pmatrix}, \quad (6)$$

such that

$$W(y) = \frac{1}{2\pi i} \int_{-\pi}^{\pi} dk_x \partial_{k_x} \log\{\det[h(k_x, y)]\}. \quad (7)$$

Here $h(k_x, y)$ is referred to as the chiral decomposition, with half the dimension of $H^{top}(k_x, y)$. Theorem (5) ensures that $g(\omega, k_x, y)$, $T(\omega = 0, k_x)$ and H_V individually admit simultaneous chiral decompositions as in Eq. (6). At $y = 0$ the topological Hamiltonian becomes $H^{top}(k_x, y = 0) = -H_V T^{-1}(0, k_x)[g(0, k_x, 0)]^{-1}$. From the chiral decomposition it follows that the winding number can be written as the sum (see Appendix B for details)

$$W(y = 0) = W_{g^{-1}(y=0)} - W_{T^{-1}} + W_{H_V}, \quad (8)$$

which is the central result of this paper. Here W_A represents of the winding number obtained from Eq. (7) with $h(k_x, y)$ replaced by the chiral decomposition of $A = [g(\omega = 0, k_x, y)]^{-1}$, $[T(\omega = 0, k_x)]^{-1}$ and H_V respectively.

In the case of a trivial substrate and trivial (including local) scattering, $W_{g^{-1}(y=0)} = W_{H_V} = 0$ and therefore

$$W(y = 0) = -W_{T^{-1}}. \quad (9)$$

The invariant only becomes undefined and changes value when $\det\{[T(\omega = 0)]^{-1}\} = 0$, matching when the in-gap bands touch.

We can also prove that the correct trivial phases are identified. Let V be the scattering strength in H_V . In the limit $V \rightarrow 0$, Eq. (8) reduces to $W(y = 0) = W_{g^{-1}(0)}$, which is trivial for a trivial substrate. In the opposite limit $V \rightarrow \infty$, we have $H^{top} \sim H_V$ and the in-gap modes are pushed to infinite energy. This Hamiltonian can no longer wind around the origin and the phase is trivial.

For a general H_V with k_x dependence, a gap closure could occur. These gap closures cause zeros in the T -matrix which can change its winding number [46]. However due to the relative negative sign between the two terms in Eq. (8), any change caused by the appearance of such a zero is perfectly compensated by the change in winding number of the scattering Hamiltonian (see Appendix B). We have therefore proven that in the case of a trivial substrate, the topological Hamiltonian proposed in [31, 32] identifies the correct trivial states and is only changed by poles of $T(\omega = 0, k_x)$. As a consequence, it indeed provides the correct topological classification when y is tuned to the interface.

The classification in the case of a topologically non-trivial substrate via the topological Hamiltonian remains outstanding though. The topological Hamiltonian H^{top} contains a dimensional reduction from a higher D dimensional substrate to a lower d dimensional interface. However, the allowed values of topological invariants changes between dimensions [48] and symmetries allowing for a non-trivial system in D dimensions may impose only trivial states in d dimensions. Therefore $[g(\omega = 0, k_x, y)]^{-1}$

does not necessarily form a good topological Hamiltonian of the substrate, whereas a trivial state remains trivial after any dimensional reduction as it remains always amenable to the atomic limit.

When $y \neq 0$, the form of the winding number becomes (see Appendix B),

$$W(y) = 2W_{g^{-1}(y)} - W_{T^{-1}} \quad (10)$$

$$- \frac{1}{2\pi i} \int_{-\pi}^{\pi} dk \partial_k \log\left\{\det[\mathbb{1} + \tilde{g}^{-1}(-y)\tilde{T}^{-1}\tilde{g}^{-1}(y)\tilde{g}(0)]\right\},$$

where $\tilde{g}^{-1}(y)$ and \tilde{T}^{-1} are the chiral decompositions of $[g(\omega = 0, k_x, y)]^{-1}$ and $[T(\omega = 0, k_x)]^{-1}$ respectively. The final term can be singular and possess non-trivial winding. As we show in Appendix B, for a trivial substrate, as $|y| \rightarrow \infty$ the zeros of $G(\omega = 0, k_x, y)$ cancel the poles of $T(\omega = 0, k_x)$ and the winding of the T -matrix is perfectly cancelled. Therefore $H^{top}(|y| \rightarrow \infty)$ is trivial. This was observed in the continuum model of a spiral magnetic interface embedded into a superconductor in Ref. [31].

Equation (8) is a general result applicable to any gapped substrate with any interface that has a chiral symmetry. We recall furthermore that it applies also to interfaces of larger width, by extending the matrix sizes to include the y coordinates of the interface too. The key appeal of this classification method is that it is calculated from analytically tractable objects, well defined in the system size $L \rightarrow \infty$ limit, removing any finite size effects. As only the local Green's function is required, this approach is applicable to first principals calculations [17–19, 38]. It also opens the door to connecting this classification to local response functions that are experimentally accessible.

Application to Magnetic Interface in a Superconductor – To demonstrate the usefulness of this approach we apply it to classify a tight-binding model as depicted in Fig. 1 of a chain of spiralling magnetic impurities embedded into a s-wave superconductor. Similarly to Refs. [8, 21, 23, 30, 31], we consider classical magnetic impurities aligned along the x direction at $y = 0$, with planar magnetisation $\mathbf{M}(x) = V_m(\cos(2k_m x), \sin(2k_m x), 0)$, where $V = V_m$ sets the scattering strength and k_m the period of the spiral. Translational symmetry along x can be restored by a gauge transformation on the electron creation operator $c_{x,y,\sigma}^\dagger \rightarrow e^{ik_m \sigma x} c_{x,y,\sigma}^\dagger$, for spin $\sigma = \uparrow, \downarrow = +, -$ [49]. This maps the magnetisation to $\mathbf{M} = V_m(1, 0, 0)$ but spin splits the bands by the shifts $k_x \rightarrow k_x + \sigma k_m$. In (k_x, y) space the components of the Hamiltonian $\mathcal{H} = \mathcal{H}_0 + \mathcal{H}_V$ are then written as

$$\mathcal{H}_0 = \sum_{k_x, y, \sigma} [-2t \cos(k_x + \sigma k_m) - \mu] c_{k_x, y, \sigma}^\dagger c_{k_x, y, \sigma}$$

$$- t \sum_{k_x, y, \sigma} \left[(c_{k_x, y+1, \sigma}^\dagger c_{k_x, y, \sigma} + \Delta c_{k_x, y, \uparrow}^\dagger c_{-k_x, y, \downarrow}^\dagger) + \text{h.c.} \right], \quad (11)$$

$$\mathcal{H}_V = V_m \sum_{k_x} c_{k_x, 0, \uparrow}^\dagger c_{k_x, 0, \downarrow} + \text{h.c.}, \quad (12)$$

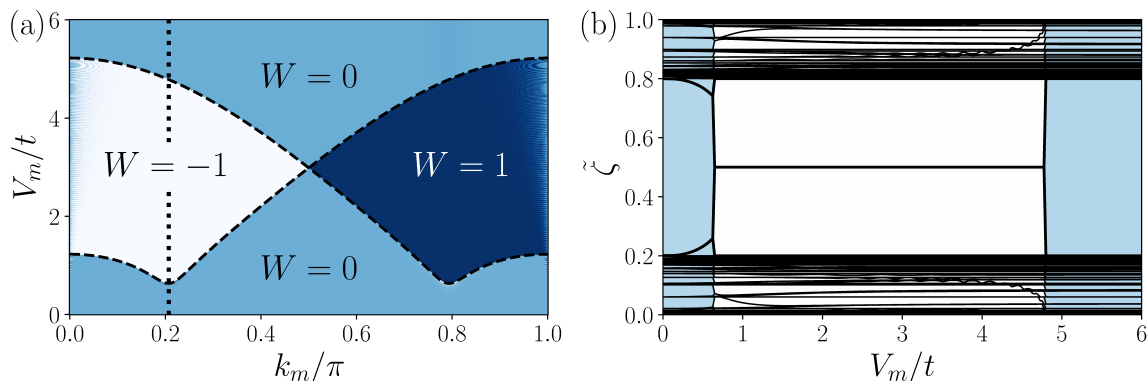


FIG. 2. (a) Winding Number of $H^{top}(k_x, y=0)$ for $\Delta = 0.1t$ and $k_F = 0.65$. Wide black dashed lines show the phase boundaries in Eq. (14). At $k_m = 0, \pi$ the model is gapless and changes symmetry class. The fuzzy pattern nearby arises from unavoidable numerical instabilities near the gap closures. The minima of the lower phase boundaries are occur at $k_m = k_F, \pi - k_F$. (b) Entanglement spectrum ζ at $k_m = k_F$ for V_m varying along the dotted line in panel (a), computed for a 50×101 lattice with an entanglement cut made perpendicular to the impurity chain splitting the system in two. The background colour indicates the winding number shown in panel (a). Edge modes, characterised by $\zeta = 1/2$, appear exactly when the winding number of the topological Hamiltonian is non-trivial.

with hopping integral t , s-wave superconductor pairing Δ , and chemical potential μ . The coordinates x, y label a square lattice with lattice constant $a = 1$. The spiral wave-vector k_m is left as a free parameter, not fixed to a free-energy minimum as in systems with effective magnetic interactions [9, 50–55]. We consider a constant Δ rather than solving self-consistently for the effect of the impurities, as this provides an almost identical phase diagram (see Appendix E) but allows for an analytic solution for the phase boundaries.

For $k_m \neq n\pi$ where $n \in \mathbb{Z}$, the model is in the BDI symmetry class [48], with chiral, particle-hole, time reversal and inversion symmetry operators [56]

$$\mathcal{C} = \tau^y \sigma^x, \quad \mathcal{P} = i\tau^x K, \quad \mathcal{T} = \tau^z \sigma^x K, \quad \mathcal{I} = \tau^z \sigma^x, \quad (13)$$

where K is the complex conjugation, and σ^i, τ^i are the Pauli matrices for spin and particle-hole degrees of freedom, respectively. The calculation of the substrate Green's function, $g(\omega, k_x, y)$, can be done as in Ref. [30] from which we obtain $T(\omega, k_x)$, as shown in Appendix C. The poles of $T(0, k_x)$ provide the gap closures of the in-gap bands that mark the topological phase boundaries. This occurs at the high symmetry points $k_x = 0, \pi$ at the scattering strengths (see Appendix D)

$$V_{m, k_x}^* = \pm \left\{ [g_{11}^\uparrow(k_x)]^2 + [g_{12}^\uparrow(k_x)]^2 \right\}^{-1/2}, \quad (14)$$

where g_{11}^\uparrow and g_{12}^\uparrow are the (\uparrow ,particle)-(\uparrow ,particle) and (\uparrow ,particle)-(\downarrow ,hole) terms of $g(\omega = 0, k_x, y = 0)$. In the continuum limit, $V_{m, k_x=0}^*$ reproduces the corresponding result of Ref. [31]. Gap closures occur only at $k_x = 0, \pi$, and so the winding number is restricted to $W = 0, \pm 1$. Using Eq. (9) the parity of the winding number of the topological Hamiltonian for $k_m \neq n\pi$ can be written as

[47]

$$(-1)^{W(y=0)} = \prod_{k_x=0, \pi} \text{sign} [(V_{m, k_x}^*)^{-2} - (V_m)^{-2}]. \quad (15)$$

Consequently a non-trivial phase is obtained for $\min(V_{m, k_x=0}^*, V_{m, k_x=\pi}^*) < V_m < \max(V_{m, k_x=0}^*, V_{m, k_x=\pi}^*)$. For $k_m = n\pi$ where $n \in \mathbb{Z}$, the spin sectors decouple and the Hamiltonian block diagonalises into two s-wave Hamiltonians with each block subject to a local Zeeman shift $V_m \sigma^z$. Each block is in the trivial CI class such that the winding number is always zero [48].

The resulting phase diagram is shown in Fig. 2(a). To further corroborate our results, in Fig. 2(b) we show the entanglement spectrum ζ as V_m is varied along the vertical dashed line in Fig. 2(a) obtained from an entanglement cut made perpendicular to the chain [57]. In a trivial phase ζ is gapped about 1/2, whereas in a non-trivial phase there is a doubly degenerate value $\zeta = 1/2$ [57]. This matches exactly our phase diagram.

Classification of Magnetic Interface Model Via Reduced Projector – The topological Hamiltonian is a local probe, but being derived from the full Green's function it carries the full information of the band structure, both bulk bands delocalised over the substrate and the in-gap bands localised to the impurity chain. Indeed Eqs. (8) and (9) involve only $y = 0$. However through T they still involve the extended bulk Green's function g , and it may be natural to ask how much involvement of the extended substrate states is actually required. As the in-gap bands are localised to the interface, it might be possible that topological properties could be completely reproducible from the wavefunctions truncated to a small wedge around the scattering interface. As this cannot be done by averaging the Hamiltonian over the y coordinate [31], we should work directly with the ground state projector. Our goal is to test under which conditions indeed

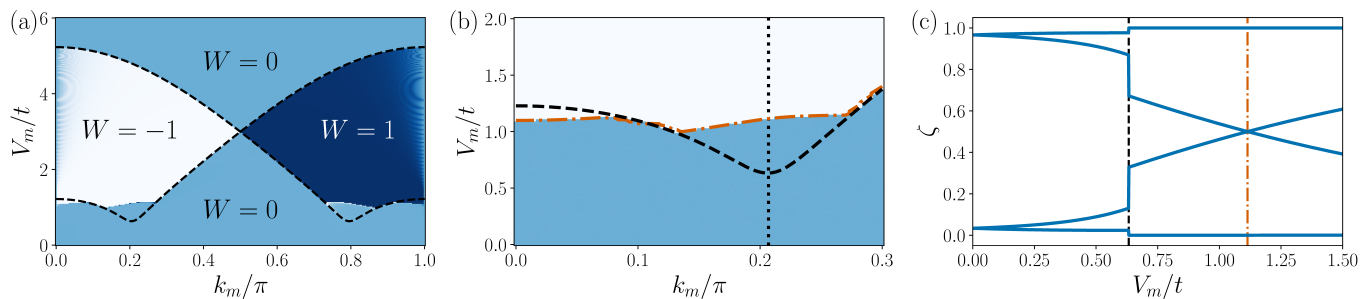


FIG. 3. (a) Winding number of $1 - 2\Pi^{\mathcal{R}}$, the projector restricted to the impurity site for $N_y = 101$, $k_F a = 0.65$ and $\Delta = 0.1t$. The black dashed lines show the phase boundaries from Eq. (14). The classification gives the incorrect topological invariant, overshooting the phase boundary for $k_m \approx 0$ and undershooting it for $k_m \approx k_F$. As in Fig. 2, the fuzzy pattern $k_m = 0, \pi$ arises from numerical instability near gap closures. (b) Same as panel (a), zoomed on $k_m \approx k_F$. The additional orange dash-dotted line shows where the gap of the projector closes, matching exactly where the winding number changes. (c) Entanglement spectrum ζ of the projector $P^{\mathcal{R}}$ reduced to just to $y = 0$, at $k_x = 0$, $k_m = k_F$ as V_m is varied along the dotted line in panel (b). The black dashed and orange dash-dotted lines mark the boundaries as in panel (b). The discontinuity in ζ (black line) mark the true phase transition, whereas the erroneous phase transition by the projector appears where the ζ gap closes instead (orange line).

the long-ranged spatial information of the substrate is of relevance. To this end we compare the results from H^{top} with the classification scheme proposed in Ref. [42] under spatial truncation.

Consider a D dimensional trivial substrate with an embedded $d < D$ dimensional topological model and ground state $|GS\rangle$ [42]. The classification scheme is based on the ground state projector [58]

$$P_{i,j}^{\alpha,\beta}(k) = \langle GS | c_{k,i,\alpha}^\dagger c_{k,j,\beta} | GS \rangle, \quad (16)$$

where k is the d dimensional momentum in the translationally invariant directions, i, j label spatial degrees of freedom in the non-translationally invariant directions, and α, β label unit cell degrees of freedom. Spatial degrees of freedom can be traced out by restricting the projector to a spatial region \mathcal{R} that contains the embedded system, leaving a reduced projector $P^{\mathcal{R}}(k)$ [59]. This projector has eigenvalues $\zeta_i(k) \in [0, 1]$ and eigenvectors $|\zeta_i(k)\rangle$. A value ζ_i near 1 refers to a state mainly supported in \mathcal{R} and a value near 0 a support mainly outside \mathcal{R} . The crossing of some ζ_i through $\zeta = 1/2$ indicates thus a qualitative change of the entanglement between \mathcal{R} and its complement and the possible topological implication can be captured through the entanglement projector [42]

$$\Pi^{\mathcal{R}}(k) = \sum_{\zeta_i(k) > 1/2} |\zeta_i(k)\rangle \langle \zeta_i(k)|, \quad (17)$$

which is in the same symmetry class as the Hamiltonian [42] and $1 - 2\Pi^{\mathcal{R}}(k)$ acts like a spectrally flattened band Hamiltonian with generally a gap about 0. Consequently it allows for the standard extraction of topological invariants [48].

An embedded topological insulator has then been defined to be the minimal spatial region such that the entanglement projector gives a non-trivial topological invariant and that any further cut causes the projector to

become gapless [42]. This is because any cut through a topological insulator that maintains protecting symmetries causes a gapless edge mode to appear in the energy and entanglement spectrum [60]. We shall show in our magnetic interface model that, though any generically spatial truncation of the y -coordinate leaves a gapped entanglement spectrum, at certain points in the phase diagram, the entanglement between \mathcal{R} and its complement can cause a gap closure in the projector, and hence if used uncritically this approach would produce an incorrect phase diagram. In this case, the truncated region is not topologically equivalent to the full embedded insulator at all points in the phase diagram.

Consider indeed the winding number of $1 - 2\Pi^{\mathcal{R}}$ for the magnetic interface model [60], with \mathcal{R} reduced to just one site at $y = 0$. This truncation leaves a generically gapped reduced projector. The result is shown in Fig. 3(a) and it does not match Fig. 2(a), overshooting the phase boundary for $k_m \approx 0$ and undershooting for $k_m \approx k_F$. This error is reproduced for larger lattice sizes and in the entanglement spectrum. To recover the correct phase diagram \mathcal{R} must be enlarged to contain ≈ 3 lattice sites on both sides of the magnetic chain. This error is particularly significant as $k_m = k_F$ arises naturally for the ground state if an effective interaction through the substrate between the magnetic impurities is taken into account [9, 50–53].

The projector's invariant can only change if the projector is discontinuous or its gap closes. The former occurs when the Hamiltonian's gap closes and the ground state reconfigures. The latter is associated with a projector eigenvalue $\zeta = 1/2$. This is a maximally entangled mode, in that it maximises the von Neumann Entropy $S = -\zeta \log(\zeta)$ [61]. As shown in Fig. 3(b,c) such modes are responsible for the erroneous phase diagram. These modes occur as the in-gap wavefunctions are spread over a few sites and have a strong entanglement between the y

and spin-Nambu degrees of freedom [31]. Thus by tracing over part of the wavefunction and only considering the central site it is possible to generate a maximally entangled state.

This result shows that the ground state projector classification requires before application a careful checking of the extent of the localised wavefunctions. Alternatively, every phase transition predicted by this method would need to be checked as to whether it is due to gap closing in the Hamiltonian or in the reduced projector. Both could become computationally costly. This underlines the significance of the role of the substrate in the dimensional reduction that is captured by a Green's function based method as put forward in this paper.

Conclusions – We have shown that the topological classification of 1D interfaces embedded into a topologically trivial 2D substrate with chiral symmetry can be performed exactly by the local Green's function tuned to the interface. With Eq. (8) we then provided an explicit formula disentangling the local scattering effects from the substrate, while maintaining the full spatial dependence of the substrate through the T -matrix. We demonstrated further that the full spatial dependence indeed is crucial for the topological classification, and care has to be taken when using classification schemes relying on a spatial truncation. Though we believe extensions into higher dimensions and non-chiral symmetry classes are possible, the proof of the applicability of a local Green's function classification to Pfaffian or Chern invariants remains outstanding. A proof for Pfaffian invariants would cover 1D Class D superconductors and would complete the classification of all non-trivial 1D symmetry classes [48, 62]. The classification of interfaces embedded into topologically non-trivial substrates with Green's function based topological Hamiltonians also requires further study.

Acknowledgements – The authors thank Joe Winter and Konner McNeillie for helpful discussions. HMS acknowledges studentship funding from EPSRC under Grant No.EP/W524505/1. The work presented in this paper is theoretical. No data were produced, and supporting research data are not required.

Appendix A: Proof of Theorem (5)

We consider the 2D substrate with the embedded scattering interface, described by the Hamiltonian $\mathcal{H}(k_x) = \mathcal{H}_0(k_x) + \mathcal{H}_V(k_x)$. The scattering interface is assumed to be concentrated to site $y = 0$, which could be a chain of impurities. Alternatively, as explained in the main text, if the interface has a larger width we can partition the y coordinates into supercells of the width of the interface, such that integer y label the position of the supercells, and the y dependence within each supercell is taken into account as internal matrix index such as spin or particle-hole degrees of freedom. For an interface in the form of a chain, the supercell matches the unit cell. Since $\mathcal{H}_V(k_x)$ is restricted to $y = 0$ we can

write $\mathcal{H}_V(k_x) = H_V(k_x) \otimes P_{y=0}$, where P_y projects onto supercell y .

Let $\{|y\rangle\}$ form an orthonormal basis of 1D wavefunctions localised at cell y such that $\langle y | \mathcal{A}(k_x) | y' \rangle$ reduces any operator $\mathcal{A}(k_x)$ to a matrix of internal degrees of freedom only. We restrict ourselves to substrates that are fully translationally invariant, so $\langle y | \mathcal{H}_0(k_x) | y' \rangle = \langle y + n | \mathcal{H}_0(k_x) | y' + n \rangle$ for all y, y', n . Consider a global symmetry of the Hamiltonian $\tilde{\Lambda}$ such that $\tilde{\Lambda}^{-1} \mathcal{H}(k_x) \tilde{\Lambda} = \pm \mathcal{H}(\pm k_x)$, where the \pm are chosen depending on the type of symmetry. As $\tilde{\Lambda}$ is global, it acts site-wise [42], i.e. the symmetry is of the form $\tilde{\Lambda} = \Lambda \otimes \mathbb{1}_y$, where Λ is an operator that acts on the degrees of freedom within a supercell and $\mathbb{1}_y$ is the identity acting on the y cell coordinate. The action of the symmetry on the Hamiltonian gives

$$\tilde{\Lambda}^{-1} [\mathcal{H}_0(k_x) + \mathcal{H}_V(k_x)] \tilde{\Lambda} = \pm [\mathcal{H}_0(\pm k_x) + \mathcal{H}_V(\pm k_x)]. \quad (\text{A1})$$

As \mathcal{H}_V is local to the interface, there exists a $y^* > 0$ such that $\langle y' | \mathcal{H}_V(k_x) | y'' \rangle = 0$ for $|y'|, |y''| > y^*$, but also that $\langle y' | \tilde{\Lambda}^{-1} \mathcal{H}_V(k_x) \tilde{\Lambda} | y'' \rangle = 0$ as $\tilde{\Lambda}$ acts only locally. Therefore for such y', y''

$$\begin{aligned} \langle y' | \tilde{\Lambda}^{-1} [\mathcal{H}_0(k_x) + \mathcal{H}_V(k_x)] \tilde{\Lambda} | y'' \rangle \\ = \pm \langle y' | [\mathcal{H}_0(\pm k_x) + \mathcal{H}_V(\pm k_x)] | y'' \rangle, \end{aligned} \quad (\text{A2})$$

reduces to

$$\langle y' | \tilde{\Lambda}^{-1} \mathcal{H}_0(k_x) \tilde{\Lambda} | y'' \rangle = \pm \langle y' | \mathcal{H}_0(\pm k) | y'' \rangle. \quad (\text{A3})$$

Due to the translational invariance of $\mathcal{H}_0(k_x)$ the latter equality holds for any y', y'' , and it follows that

$$\tilde{\Lambda}^{-1} \mathcal{H}_0(k_x) \tilde{\Lambda} = \pm \mathcal{H}_0(\pm k). \quad (\text{A4})$$

This means that $\tilde{\Lambda}$ is a symmetry for $\mathcal{H}_0(k_x)$ separately too. From Eq. (A1) it follows in turn that

$$\tilde{\Lambda}^{-1} \mathcal{H}_V(k_x) \tilde{\Lambda} = \pm \mathcal{H}_V(\pm k), \quad (\text{A5})$$

so that $\tilde{\Lambda}$ is a symmetry also for $\mathcal{H}_V(k_x)$. It follows further that Λ is a symmetry of $H_V(k_x)$.

Finally from Eq. (4) in the main text, we obtain that if $\tilde{\Lambda}$ is a symmetry of $\mathcal{H}_0(k_x)$, then Λ is a symmetry of $g(\omega = 0, k_x, y)$.

To prove the converse let us assume that Λ is a symmetry of $g(\omega = 0, k_x, y)$. Then $\tilde{\Lambda} = \Lambda \otimes \mathbb{1}_y$ is a symmetry of $\mathcal{H}_0(k_x)$ for the translationally invariant substrate. If furthermore Λ is a symmetry of $H_V(k_x)$, then $\tilde{\Lambda}$ is a symmetry of $\mathcal{H}_V(k_x) = H_V(k_x) \otimes P_{y=0}$. Therefore from Eq. (A1), $\tilde{\Lambda}$ is a symmetry of $\mathcal{H}(k_x)$. This concludes the proof of Theorem (5).

Appendix B: Winding Number of Topological Hamiltonian

The winding number can be evaluated by writing the Dyson equation for Green's function [Eq. (1) in the main

text] as follows

$$G(0, k_x, y, y') = g(0, k_x, y)T(0, k_x)g(0, k_x, -y') \\ \times \left\{ \mathbb{1} + [g(0, k_x, -y')]^{-1} [T(0, k_x)]^{-1} \right. \\ \left. \times [g(0, k_x, y)]^{-1} g(0, k_x, 0) \right\}. \quad (\text{B1})$$

where $\mathbb{1}$ is the identity operator, the y label supercells as explained in Sec. A, and the written G, g and T are matrices in all internal degrees of freedom of a supercell. The inversion of the substrate Green's function and the T -matrix is possible due to the assumption that both are gapped apart from at phase boundaries. The topological Hamiltonian [Eq. (3) in the main text] can then be written as

$$H^{top}(k_x, y) = - \left\{ \mathbb{1} + [g(0, k_x, -y)]^{-1} [T(0, k_x)]^{-1} \right. \\ \left. \times [g(0, k_x, y)]^{-1} g(0, k_x, 0) \right\}^{-1} \\ \times [g(0, k_x, -y)]^{-1} [T(0, k_x)]^{-1} [g(0, k_x, y)]^{-1}. \quad (\text{B2})$$

To simplify the notation we shall omit the index k_x in most of the following expressions.

1. Case $y = 0$

Let us consider $y = 0$ and set $g = g(0, k_x, 0)$ and $T = T(0, k_x)$. The topological Hamiltonian then becomes

$$H^{top}(k_x) = -(\mathbb{1} + g^{-1}T^{-1})^{-1} g^{-1}T^{-1}g^{-1} \\ = -[\mathbb{1} + g^{-1}(H_V^{-1} - g)]^{-1} g^{-1}T^{-1}g^{-1} \\ = -H_V T^{-1} g^{-1}. \quad (\text{B3})$$

Theorem (5) guarantees that T, g and H_V , and therefore H^{top} , are all chiral symmetric, admit a simultaneous chiral decomposition, and can be written in the chiral eigenbasis

$$H_V = \begin{pmatrix} 0 & h_V \\ h_V^\dagger & 0 \end{pmatrix}, \quad g^{-1} = \begin{pmatrix} 0 & \tilde{g}^{-1} \\ \tilde{g}^{-1\dagger} & 0 \end{pmatrix}, \\ T^{-1} = \begin{pmatrix} 0 & \tilde{T}^{-1} \\ \tilde{T}^{-1\dagger} & 0 \end{pmatrix}, \quad H^{top} = \begin{pmatrix} 0 & h^{top} \\ h^{top\dagger} & 0 \end{pmatrix}, \quad (\text{B4})$$

where

$$h^{top} = -h_V \tilde{T}^{-1\dagger} \tilde{g}^{-1}. \quad (\text{B5})$$

The minus sign does not affect the winding number which can then be evaluated as

$$W(y=0) = \frac{1}{2\pi i} \int_{-\pi}^{\pi} dk_x \partial_{k_x} \log[\det(h^{top})] \\ = \frac{1}{2\pi i} \int_{-\pi}^{\pi} dk_x \partial_{k_x} \left\{ \log[\det(h_V)] + \log[\det(\tilde{T}^{-1\dagger})] \right. \\ \left. + \log[\det(\tilde{g}^{-1})] \right\}. \quad (\text{B6})$$

Consider a general chiral symmetric operator A with chiral decomposition a and take a change of variable $z = \det(a)$ such that the k_x integration over the first Brillouin zone becomes the z integration over the closed contour $\mathcal{Z} = \{z = \det(a(k_x)) | k_x \in [-\pi, \pi)\}$. We can then write the corresponding winding number in the form

$$W_A = \int_{-\pi}^{\pi} \frac{dk_x}{2\pi i} \partial_{k_x} \log\{\det[a(k_x)]\} = \oint_{\mathcal{Z}} \frac{dz}{2\pi i z}. \quad (\text{B7})$$

From this expression we see that if we take $a \rightarrow a^\dagger$, $\det(a) \rightarrow \det(a)^*$ then \mathcal{Z} is inverted about the real axis and the contour is traversed in the opposite direction. This gives an overall minus to the winding number. Therefore the winding number of the topological Hamiltonian becomes

$$W(y=0) = W_{g^{-1}} - W_{T^{-1}} + W_{H_V}. \quad (\text{B8})$$

A locally acting H_V has a zero winding number. But general k_x dependent $H_V(k_x)$ may lead to $W_{H_V} \neq 0$, and thus seemingly to a topological phase transition without gap closure. However, in such a case the change in W_{H_V} is compensated by a simultaneous change in $W_{T^{-1}}$, so that a gap closure still remains mandatory. To see this, we should recall that $-W_{T^{-1}} + W_{H_V}$ represents the winding of $H_V T^{-1} = \mathbb{1} - H_V g$, thus of $\det(\mathbb{1} - h_V \tilde{g}^\dagger)$. This means that the direct winding from H_V is undone but the zeros of T^{-1} are preserved. In case of doubt indeed the foolproof expression to be used for the winding number is $(\mathbb{1} - h_V \tilde{g}^\dagger)$, whereas the T -matrix arises naturally from scattering theory and remains under normal conditions the object of choice.

2. Case $y \neq 0$

When $y \neq 0$, the chiral decomposition of the Hamiltonian is

$$h^{top}(y) = - \left\{ \mathbb{1} + [\tilde{g}(-y)]^{-1} \tilde{T}^{-1\dagger} [\tilde{g}(y)]^{-1} \tilde{g}(0) \right\}^{-1} \\ \times [\tilde{g}(-y)]^{-1} \tilde{T}^{-1\dagger} [\tilde{g}(y)]^{-1}, \quad (\text{B9})$$

where $\tilde{g}(y)$ is the chiral decomposition of $g(0, k_x, y)$. The winding number is then evaluated as before. We obtain

$$W(y) = \int_{-\pi}^{\pi} \frac{dk_x}{2\pi i} \\ \times \partial_k \left\{ -\log[\det(\mathbb{1} + [\tilde{g}(-y)]^{-1} \tilde{T}^{-1\dagger} [\tilde{g}(y)]^{-1} \tilde{g}(0))] \right. \\ \left. + \log[\det([\tilde{g}(-y)]^{-1})] + \log[\det(\tilde{T}^{-1\dagger})] \right. \\ \left. + \log[\det([\tilde{g}(y)]^{-1})] \right\}, \quad (\text{B10})$$

which gives Eq. (10) in the main text. If we consider the Lehmann representation of the Green's function [43]

$$G(\omega, k_x) = \sum_n \frac{|E_n(k_x)\rangle \langle E_n(k_x)|}{\omega_+ - E_n(k_x)}, \quad (\text{B11})$$

where E_n and $|E_n\rangle$ are the eigenvalues and eigenmodes of the Hamiltonian and $\omega_+ = \omega + i0^+$, the local Green's function can be written as

$$G(\omega, k_x, y, y) = \langle y | G(\omega, k_x) | y \rangle \\ = \sum_n \frac{\langle y | E_n(k_x) \rangle \langle E_n(k_x) | y \rangle}{\omega_+ - E_n(k_x)}. \quad (\text{B12})$$

For a trivial substrate the in-gap wavefunctions are localised to the interface region and normalisable. Therefore for such wavefunctions $\lim_{|y| \rightarrow \infty} \langle y | E_{in-gap}(k_x) \rangle = 0$. Taking thus $|y| \rightarrow \infty$ for generic V_m, k_m suppresses any pole from the in-gap modes. The remaining poles are from substrate and therefore gapped as the substrate is trivial. This then means that $W(|y| \rightarrow \infty) = 0$ and $H^{top}(k_x, |y| \rightarrow \infty)$ is trivial. Examining the form of the winding number we obtain

$$W_{T^{-1}} = - \lim_{|y| \rightarrow \infty} \int_{-\pi}^{\pi} \frac{dk_x}{2\pi i} \\ \times \partial_k \log \left\{ \det \left[\mathbb{1} + [\tilde{g}(-y)]^{-1} \tilde{T}^{-1\dagger} [\tilde{g}(y)]^{-1} \tilde{g}(0) \right] \right\}. \quad (\text{B13})$$

From the form of the Green's function in Eq. (B1) we see the term that gives the y dependent winding number does not have any poles (as we have assumed the substrate is trivial). As such any change in the winding number as y is varied must be due to zeros in the determinant of this term and so of $G(\omega = 0, k_x, y, y)$.

Appendix C: Fourier transform of lattice s-wave superconductor Green's function

The partially Fourier transformed retarded Green's function of a square lattice s-wave superconductor is evaluated. The Hamiltonian of such a 2D superconductor, after taking the gauge transformation $c_{x,y,\sigma}^\dagger \rightarrow e^{ik_m \sigma} c_{x,y,\sigma}^\dagger$, where k_m is the spiral wavevector of the magnetic impurity interface, is given by

$$\mathcal{H}_0(k_x, k_y) = \mathcal{H}^\dagger \sigma^\uparrow + \mathcal{H}^\downarrow \sigma^\downarrow, \quad (\text{C1})$$

where we define $\sigma^{\uparrow,\downarrow} = (\mathbb{1} \pm \sigma^z)/2$, for σ^z the Pauli- z matrix acting on the spin degrees of freedom and

$$\mathcal{H}^\sigma = \epsilon_{k_x, k_y, \sigma} \tau^z + \sigma \Delta \tau^x, \quad (\text{C2})$$

where $\epsilon_{k_x, k_y, \sigma} = -2t(\cos(k_x + \sigma k_m) + \cos(k_y)) - \mu$, the τ^i are the Pauli matrices acting on the particle-hole degrees of freedom, t is the hopping integral, μ the chemical potential, and Δ the superconductor pairing amplitude chosen to be real and positive. The retarded Green's function of the superconductor is given by [43]

$$g(\omega, k_x, k_y) = [\omega_+ - \mathcal{H}_0(k_x, k_y)]^{-1}, \quad (\text{C3})$$

where $\omega_+ = \omega + i0^+$. The partial Fourier transform of the retarded Green's function is defined as [30]

$$g(\omega, k_x, y) = \int_{-\pi}^{\pi} \frac{dk_y}{2\pi} e^{ik_y y} g(\omega, k_x, k_y). \quad (\text{C4})$$

For the given Hamiltonian we obtain

$$g(\omega, k_x, y) = g^\uparrow(\omega, k_x, y) \sigma^\uparrow + g^\downarrow(\omega, k_x, y) \sigma^\downarrow, \quad (\text{C5})$$

with

$$g^\sigma(\omega, k_x, y) = \frac{1}{2\pi} \int_{-\pi}^{\pi} dk_y \frac{e^{ik_y y} (\omega_+ + \epsilon_{k_x, \sigma} \tau^z + \sigma \Delta \tau^x)}{\omega_+^2 - \epsilon_{k_x, \sigma}^2 - \Delta^2}. \quad (\text{C6})$$

We should notice that since $g(\omega, k_x, k_y) = g(\omega, k_x, -k_y)$ this integral is independent of the sign of y and we can thus replace $y \rightarrow |y|$. We then change the integration variable to $z = e^{ik_y}$, with $dz = iz dk_y$, such that the integration is over the unit circle S^1 in the positive, anticlockwise direction, and obtain

$$g^\sigma(\omega, k_x, y) = \frac{1}{2\pi i} \oint_{S^1} dz z^{|y|-1} g(\omega, k_x, z). \quad (\text{C7})$$

As we focus on the in-gap states with $|\omega| < \Delta$, the small $+i0^+$ is of no importance we shall use ω instead of ω_+ henceforth. Focusing on just the denominator in the integrand

$$z(\omega^2 - \epsilon_{k_x, z, \sigma}^2 - \Delta^2) \\ = z \left\{ \omega^2 - [-t(z + 1/z) - \mu_{k_x}]^2 - \Delta^2 \right\} \\ = z(\omega^2 - \Delta^2) - \frac{z}{z^2} [t(z^2 + 1) + \mu_{k_x} z]^2 \\ = \frac{t^2}{z} \left\{ z^2(\tilde{\omega}^2 - \tilde{\Delta}^2) - [(z^2 + 1) + \tilde{\mu}_{k_x} z]^2 \right\}, \quad (\text{C8})$$

where we have defined $\tilde{\mu}_{k_x} = \tilde{\mu} + 2 \cos(k_x + \sigma k_m)$ and introduced the dimensionless energies $\tilde{\omega} = \omega/t$, $\tilde{\Delta} = \Delta/t$, and $\tilde{\mu} = \mu/t$. The integral then becomes

$$g^\sigma(\omega, k_x, y) = \frac{1}{2\pi i t^2} \oint_{S^1} \frac{dz z^{|y|+1} g^\sigma(\omega, k_x, z)}{z^2(\tilde{\omega}^2 - \tilde{\Delta}^2) - [(z^2 + 1) + \tilde{\mu}_{k_x} z]^2}. \quad (\text{C9})$$

The numerator is given by

$$z^{|y|+1} g^\sigma(\omega, k_x, z) = t z^{|y|} \left[\tilde{\omega} z - (\tilde{\mu}_{k_x} z + z^2 + 1) \tau^z + z \sigma \tilde{\Delta} \tau^x \right]. \quad (\text{C10})$$

All the poles are contained within the denominator and we can safely proceed by solving

$$0 = z^2(\tilde{\omega}^2 - \tilde{\Delta}^2) - [(z^2 + 1) + \tilde{\mu}_{k_x} z]^2, \quad (\text{C11})$$

or

$$z^2(\tilde{\omega}^2 - \tilde{\Delta}^2) = [(z^2 + 1) + \tilde{\mu}_{k_x} z]^2, \quad (\text{C12})$$

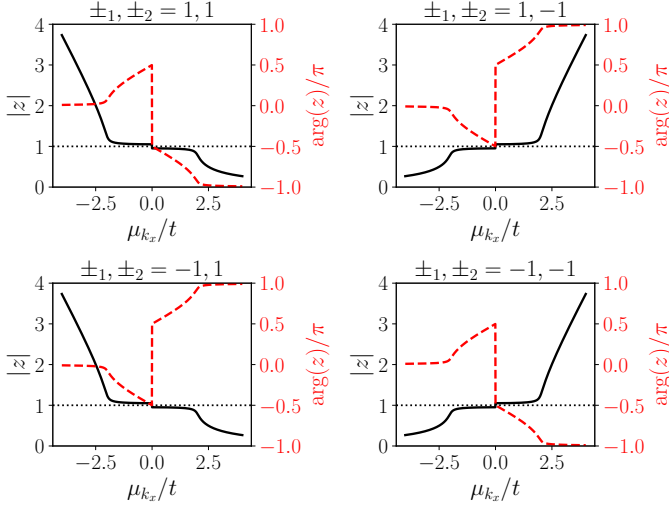


FIG. 4. Modulus (black, solid) and phase (red, dashed) of the poles obtained from Eq. (C13) for $\omega = 0$ and $\Delta = 0.1t$. The black dotted line shows $|z| = 1$. One can verify that as long as $|\omega| < \Delta$, the two poles $z_{\pm, \text{sign}(\mu_{k_x})}$ are within in the unit circle.

from which the square root leads to the two quadratic equations

$$0 = z^2 + z(\tilde{\mu}_{k_x} \pm \sqrt{\tilde{\omega}^2 - \tilde{\Delta}^2}) + 1. \quad (\text{C13})$$

We thus obtain the four roots of the denominator

$$z_{\pm 1, \pm 2} = \frac{1}{2} \left[\tilde{\mu}_{k_x} \pm 1 \sqrt{\tilde{\omega}^2 - \tilde{\Delta}^2} \right] \pm \frac{1}{2} \sqrt{\left(-\tilde{\mu}_{k_x} \pm 1 \sqrt{\tilde{\omega}^2 - \tilde{\Delta}^2} \right)^2 - 4}. \quad (\text{C14})$$

Then the integral is

$$g^\sigma(\omega, k_x, y) = \frac{-1}{2\pi i t} \oint_{S^1} \frac{z^{|y|} dz}{(z - z_{+,+})(z - z_{-,+})(z - z_{+,-})(z - z_{-,-})} \times \left[\tilde{\omega}z - (\tilde{\mu}_{k_x} z + z^2 + 1)\tau^z + z\sigma\tilde{\Delta}\tau^x \right]. \quad (\text{C15})$$

The total minus sign arises from the negative z^4 coefficient in the denominator. The integral can then be evaluated using Cauchy's residue theorem. In Fig. 4 we show the value of the poles for the example of $\omega = 0$ as a function of μ_{k_x} . For $|\omega| < \Delta$ the poles $z_{1,2} = z_{\pm, \text{sign}(\mu_k)}$ lie within the unit circle, and the poles $z_{3,4} = z_{\pm, -\text{sign}(\mu_k)}$ are outside the unit circle. The Green's function then evaluates to

$$g^\sigma(\omega, k_x, y) = \frac{-\xi_+(\tilde{\omega} + \sigma\tilde{\Delta}\tau^x) + i\xi_-\sqrt{\tilde{\Delta}^2 - \tilde{\omega}^2}\tau^z}{t(z_1 - z_2)} \quad (\text{C16})$$

where

$$\xi_{\pm} = \frac{z_1^{|y|+1}}{(z_1 - z_3)(z_1 - z_4)} \pm \frac{z_2^{|y|+1}}{(z_2 - z_3)(z_2 - z_4)}. \quad (\text{C17})$$

We note that ξ_+ is real and ξ_- purely imaginary as $z_1 = z_2^*$ and $z_3 = z_4^*$. Consequently g^σ is real as expected for a Green's function when ω lies in a range with vanishing density of states. The ξ_{\pm} functions are non-singular as long as $\Delta \neq 0$. We emphasise that this is the exact Green's function of a square lattice tight binding s-wave superconductor, and no low-energy approximation has been made.

Appendix D: Phase Diagram

With the explicit form of the Green's function for the impurity chain given by Eq. (1) in the main text, we can solve for the conditions of a phase boundary by finding poles of the T -matrix at $\omega = 0$,

$$\det[T^{-1}(0, k_x)] = 0. \quad (\text{D1})$$

This equation can be simplified by making use the model's chiral symmetry at $\omega = 0$. We can write the T -matrix in the eigenbasis of the chiral symmetry, using the unitary

$$U = \frac{1}{\sqrt{2}} \begin{pmatrix} 1 & 0 & 1 & 0 \\ 0 & i & 0 & i \\ 0 & -1 & 0 & 1 \\ i & 0 & -i & 0 \end{pmatrix}, \quad (\text{D2})$$

written in the basis

$$(c_{k_x, y=0, \uparrow}, c_{k_x, y=0, \downarrow}, c_{-k_x, y=0, \uparrow}^\dagger, c_{-k_x, y=0, \downarrow}^\dagger). \quad (\text{D3})$$

This transforms the T -matrix to

$$U^\dagger T^{-1} U = \begin{pmatrix} 0 & \tilde{T}^{-1} \\ \tilde{T}^{-1\dagger} & 0 \end{pmatrix}, \quad (\text{D4})$$

with the notation $T = T(\omega = 0, k_x)$ and

$$\det(T^{-1}) = |\det(\tilde{T}^{-1})|^2. \quad (\text{D5})$$

Defining the notation $g_{ij}^\sigma = [g^\sigma(\omega = 0, k_x, y = 0)]_{ij}$ and using that at $\omega = 0$ we have $g_{11}^\sigma = -g_{22}^\sigma$ and $g_{12}^\sigma = g_{21}^\sigma$, we obtain

$$\tilde{T}^{-1} = \begin{pmatrix} ig_{12}^\uparrow - g_{11}^\uparrow & \frac{i}{v_m} \\ -\frac{i}{v_m} & ig_{12}^\downarrow - g_{11}^\downarrow \end{pmatrix}. \quad (\text{D6})$$

The condition for a phase transition is $\det(T^{-1}) = 0$, which becomes

$$0 = g_{11}^\uparrow g_{11}^\downarrow - g_{12}^\uparrow g_{12}^\downarrow - i(g_{11}^\uparrow g_{12}^\downarrow + g_{11}^\downarrow g_{12}^\uparrow) - \frac{1}{v_m^2}. \quad (\text{D7})$$

The bare Green's function is real as the density of states is zero at $\omega = 0$, and as noted earlier we can omit the infinitesimal shifts $i0^+$. Then the real and imaginary parts split into two equations. The imaginary part gives

$$g_{11}^\downarrow g_{12}^\uparrow = -g_{11}^\uparrow g_{12}^\downarrow. \quad (\text{D8})$$

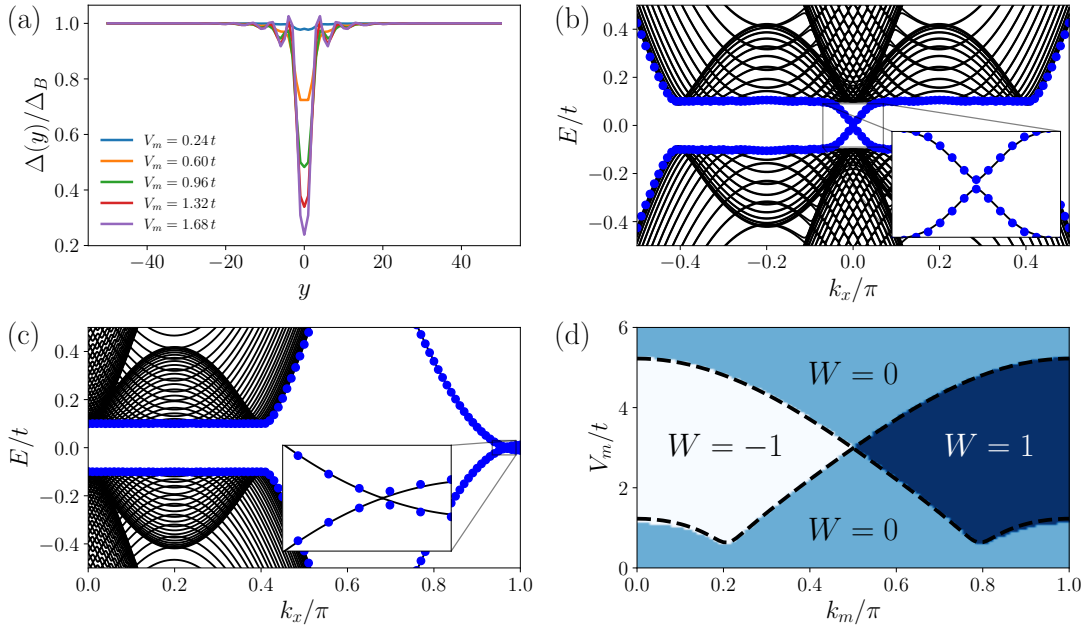


FIG. 5. Results of self-consistent calculations for $N_y = 101$, $\Delta_B = 0.1t$ and $k_F = 0.65$. Panel (a) Shows $\Delta(y)$ for $k_m = k_F$ and various values of V_m . Although the scattering potential has a considerable effect at the impurity site at $y = 0$, the renormalisation of $\Delta(y)$ almost immediately drops to below 10% independently of the scattering strength. Panels (b) and (c) show a comparison of the band structure of the self-consistent solution (black lines) and lowest two eigenvalues of the non-self consistent $\Delta(y) = \Delta_B$ (blue circles) for $k_m = 0.63$, and $V_m = 0.6$ and 4.8 respectively. There is very little difference between the two, particularly around the gap closures at $k_x = 0, \pi$. The insets confirm that there is little change in the electronic structure. Panel (d) shows the phase diagram obtained from Eq. (E3) together with the analytically calculated phase boundaries from Eq. (14). There is almost perfect agreement.

If $k_m \neq n\pi$ for $n \in \mathbb{Z}$, this has solutions for any set of system parameters, but required $k_x = 0, \pi$. This is because the only differences between the two spin species is the kinetic energy $\cos(k_x + \sigma k_m)$ and the sign of the pairing $\sigma\Delta$. At $k_x = 0, \pi$, the dispersions are equal as $\cos(k_x + \sigma k_m) = \pm \cos(\sigma k_m) = \pm \cos(k_m)$. Therefore $g_{11}^\uparrow = g_{11}^\downarrow$ and $g_{12}^\uparrow = -g_{12}^\downarrow$, and so the above equation is satisfied. When $k_m = 0, \pi$, the above equation is satisfied for any k_x meaning the gap closes and stays closed rather than opening up again.

The real part gives the conditions for the phase transition and along with the symmetry of the spin species at $k_x = 0, \pi$. We find

$$V_{m,k_x}^* = \pm \left\{ [g_{11}^\uparrow(k_x)]^2 + [g_{12}^\uparrow(k_x)]^2 \right\}^{-1/2}. \quad (\text{D9})$$

giving Eq. (14) in the main text. As gap closures only occur at $k_x = 0, \pi$, the winding number is restricted to $W = 0, 1, -1$ and therefore it is sufficient to find its parity. This can be written as the sign of the product of the determinants of the chiral decomposition at $k_x = 0, \pi$ [47]. Using the chiral decomposition above, this is given

by

$$\begin{aligned} (-1)^{W(y=0)} &= \prod_{k_x=0,\pi} \text{sign} \left[(g_{11}^\uparrow)^2 + (g_{12}^\uparrow)^2 - (V_m)^{-2} \right] \\ &= \prod_{k_x=0,\pi} \text{sign} \left[(V_{m,k_x}^*)^{-2} - (V_m)^{-2} \right], \end{aligned} \quad (\text{D10})$$

giving Eq. (15) in the main text.

Appendix E: Phase Diagram of Self-Consistent Solution

We describe a self-consistent solution to the superconducting gap equations in the presence of a magnetic interface and show that it makes very little difference to the overall phase diagram. The self-consistency condition is the same that was used in Ref. [30, 31]. We restrict ourselves to just s-wave pairing as the triplet pairing is extremely weak. We maintain translational invariance along the x -direction. Then the self consistency condition is

$$\Delta(y) = V_P \langle c_{x,y,\uparrow}^\dagger c_{x,y,\downarrow}^\dagger \rangle = V_P \sum_{k_x} \langle c_{k_x,y,\uparrow}^\dagger c_{-k_x,y,\downarrow}^\dagger \rangle, \quad (\text{E1})$$

where $\langle \dots \rangle$ denotes the ground state average. The translational invariance along the x -direction means the pairing is only a function of y . The pairing potential strength V_P is chosen such that the pairing tends to the chosen bulk pairing, Δ_B (i.e. the pairing at $V_m = 0$)

$$V_P = \frac{\Delta_B}{\sum_{k_x} \langle c_{k_x, |y| \rightarrow \infty, \uparrow}^\dagger c_{-k_x, |y| \rightarrow \infty, \downarrow} \rangle}. \quad (\text{E2})$$

Starting from the initial guess $\Delta(y) = \Delta_B$ we calculate $\langle c_{k_x, y, \uparrow}^\dagger c_{-k_x, y, \downarrow} \rangle$ from direct diagonalisation of the tight-binding matrix. With this result we update V_P through Eq. (E2) to guarantee that $\Delta(y)$ tends to Δ_B at large y . With this we reconstruct the Hamiltonian and iterate until convergence. With the final solution of the tight-binding model we calculate a topological invariant of the bands. As it is computationally heavy to calculate the winding number of a large matrix, we make use of the inversion symmetry to calculate an equivalent invariant. This is defined as

$$\nu = n_0 - n_\pi, \quad (\text{E3})$$

where n_{k_x} is the number of negative non-zero eigenvalues of $P(k_x)\mathcal{I}P(k_x)$ where \mathcal{I} is the inversion symmetry operator. This has been shown to be equal to the number of $\zeta = 1/2$ modes in the entanglement spectrum localised to the edge of the system [57].

The self consistent solution to the gap is shown in Fig. 5(a) for various V_m . We see that the gap is lowered by around 20% around the magnetic impurity around the critical scattering $V_{m, k_x=0}^* \approx 0.63t$. The residual error of this solution is on the order of $10^{-8}\Delta_B$. We show the band structure for two values of V_m around the phase boundaries in Fig. 5(b)–(c) and compare it to the in-gap bands of the non-self-consistent solution. We again see that around the bottom of the band very little difference is made and the only visible deviations are around the $k_x \approx 2k_F$ where the in-gap bands of the self-consistent solution are slightly lower than the non-self-consistent one. Finally, in Fig. 5(d) we show the phase diagram of the invariant ν defined above with the non-self-consistent phase boundaries overlaid and again we see perfectly agreement up to the pixel size. We conclude that self-consistency has so little effect on all relevant results such that it can be safely ignored.

-
- [1] A. Y. Kitaev, Unpaired Majorana fermions in quantum wires, *Physics-Uspekhi* **44**, 131 (2001).
 - [2] N. Read and D. Green, Paired states of fermions in two dimensions with breaking of parity and time-reversal symmetries and the fractional quantum Hall effect, *Physical Review B* **61**, 10267 (2000).
 - [3] M. Sato and Y. Ando, Topological superconductors: a review, *Reports on Progress in Physics* **80**, 076501 (2017).
 - [4] A. Y. Kitaev, Fault-tolerant quantum computation by anyons, *Annals of Physics* **303**, 2 (2003).
 - [5] J. K. Pachos, *Introduction to Topological Quantum Computation* (Cambridge University Press, 2012).
 - [6] M. M. Sharma, P. Sharma, N. K. Karn, and V. P. S. Awana, Comprehensive review on topological superconducting materials and interfaces, *Superconductor Science and Technology* **35**, 083003 (2022).
 - [7] Y. Oreg, G. Refael, and F. Von Oppen, Helical liquids and Majorana bound states in quantum wires, *Physical Review Letters* **105**, 177002 (2010).
 - [8] S. Nadj-Perge, I. K. Drozdov, B. A. Bernevig, and A. Yazdani, Proposal for realizing Majorana fermions in chains of magnetic atoms on a superconductor, *Physical Review B* **88**, 020407 (2013).
 - [9] I. Reis, D. J. J. Marchand, and M. Franz, Self-organized topological state in a magnetic chain on the surface of a superconductor, *Physical Review B* **90**, 085124 (2014).
 - [10] T. Meng, J. Klinovaja, S. Hoffman, P. Simon, and D. Loss, Superconducting gap renormalization around two magnetic impurities: From Shiba to Andreev bound states, *Physical Review B* **92**, 064503 (2015).
 - [11] L. Yu, Bound state in superconductors with paramagnetic impurities, *Acta Physica Sinica* **21**, 75 (1965).
 - [12] H. Shiba, Classical spins in superconductors, *Progress of Theoretical Physics* **40**, 435 (1968).
 - [13] A. Rusinov, Superconductivity near a paramagnetic impurity, *JETP Lett.* **9**, 85 (1969).
 - [14] M. H. Christensen, M. Schecter, K. Flensberg, B. M. Andersen, and J. Paaske, Spiral magnetic order and topological superconductivity in a chain of magnetic adatoms on a two-dimensional superconductor, *Physical Review B* **94**, 144509 (2016).
 - [15] T.-P. Choy, J. M. Edge, A. R. Akhmerov, and C. W. J. Beenakker, Majorana fermions emerging from magnetic nanoparticles on a superconductor without spin-orbit coupling, *Physical Review B* **84**, 195442 (2011).
 - [16] J. Li, H. Chen, I. K. Drozdov, A. Yazdani, B. A. Bernevig, and A. H. MacDonald, Topological superconductivity induced by ferromagnetic metal chains, *Physical Review B* **90**, 235433 (2014).
 - [17] B. Nyári, A. Lászlóffy, G. Csire, L. Szunyogh, and B. Újfalussy, Topological superconductivity from first principles. I. Shiba band structure and topological edge states of artificial spin chains, *Physical Review B* **108**, 134512 (2023).
 - [18] A. Lászlóffy, B. Nyári, G. Csire, L. Szunyogh, and B. Újfalussy, Topological superconductivity from first principles. II. Effects from manipulation of spin spirals: Topological fragmentation, braiding, and quasi-Majorana bound states, *Physical Review B* **108**, 134513 (2023).
 - [19] D. Sticlet and C. Morari, Topological superconductivity from magnetic impurities on monolayer NbSe₂, *Physical Review B* **100**, 075420 (2019).
 - [20] C. Mier, D.-J. Choi, and N. Lorente, Calculations of in-gap states of ferromagnetic spin chains on s-wave wide-band superconductors, *Physical Review B* **104**, 245415 (2021).
 - [21] F. Pientka, L. I. Glazman, and F. von Oppen, Topological

- superconducting phase in helical Shiba chains, *Physical Review B* **88**, 155420 (2013).
- [22] F. Pientka, L. I. Glazman, and F. Von Oppen, Unconventional topological phase transitions in helical Shiba chains, *Physical Review B* **89**, 180505 (2014).
- [23] A. Westström, K. Pöyhönen, and T. Ojanen, Topological properties of helical Shiba chains with general impurity strength and hybridization, *Physical Review B* **91**, 064502 (2015).
- [24] P. M. R. Brydon, S. Das Sarma, H.-Y. Hui, and J. D. Sau, Topological Yu-Shiba-Rusinov chain from spin-orbit coupling, *Physical Review B* **91**, 064505 (2015).
- [25] A. Heimes, P. Kotetes, and G. Schön, Majorana fermions from Shiba states in an antiferromagnetic chain on top of a superconductor, *Physical Review B* **90**, 060507 (2014).
- [26] K. Pöyhönen, A. Westström, and T. Ojanen, Topological superconductivity in ferromagnetic atom chains beyond the deep-impurity regime, *Physical Review B* **93**, 014517 (2016).
- [27] G. M. Andolina and P. Simon, Topological properties of chains of magnetic impurities on a superconducting substrate: Interplay between the Shiba band and ferromagnetic wire limits, *Physical Review B* **96**, 235411 (2017).
- [28] Y. Peng, F. Pientka, L. I. Glazman, and F. Von Oppen, Strong localization of Majorana end states in chains of magnetic adatoms, *Physical Review Letters* **114**, 106801 (2015).
- [29] Q.-H. Wang and Z. D. Wang, Impurity and interface bound states in $d_{x^2-y^2} + id_{xy}$ and $p_x + ip_y$ superconductors, *Physical Review B* **69**, 092502 (2004).
- [30] C. J. F. Carroll and B. Braunecker, Subgap states at ferromagnetic and spiral-ordered magnetic chains in two-dimensional superconductors. I. Continuum description, *Physical Review B* **104**, 245133 (2021).
- [31] C. J. F. Carroll and B. Braunecker, Subgap states at ferromagnetic and spiral-ordered magnetic chains in two-dimensional superconductors. II. Topological classification, *Physical Review B* **104**, 245134 (2021).
- [32] N. Sedlmayr, V. Kaladzhyan, and C. Bena, Analytical and semianalytical tools to determine the topological character of Shiba chains, *Physical Review B* **104**, 024508 (2021).
- [33] N. Sedlmayr and C. Bena, Instability of Majorana states in Shiba chains due to leakage into a topological substrate, *Journal of Physics: Condensed Matter* **34**, 104004 (2022).
- [34] S. Nadj-Perge, I. K. Drozdov, J. Li, H. Chen, S. Jeon, J. Seo, A. H. MacDonald, B. A. Bernevig, and A. Yazdani, Observation of Majorana fermions in ferromagnetic atomic chains on a superconductor, *Science* **346**, 602 (2014).
- [35] M. Ruby, F. Pientka, Y. Peng, F. Von Oppen, B. W. Heinrich, and K. J. Franke, End states and subgap structure in proximity-coupled chains of magnetic adatoms, *Physical Review Letters* **115**, 197204 (2015).
- [36] G. C. Ménard, S. Guissart, C. Brun, S. Pons, V. S. Stolyarov, F. Debontridder, M. V. Leclerc, E. Janod, L. Cario, D. Roditchev, P. Simon, and T. Cren, Coherent long-range magnetic bound states in a superconductor, *Nature Physics* **11**, 1013 (2015).
- [37] R. Pawlak, M. Kisiel, J. Klinovaja, T. Meier, S. Kawai, T. Glatzel, D. Loss, and E. Meyer, Probing atomic structure and Majorana wavefunctions in mono-atomic Fe chains on superconducting Pb surface, *npj Quantum Information* **2**, 1 (2016).
- [38] B. E. Feldman, M. T. Randeria, J. Li, S. Jeon, Y. Xie, Z. Wang, I. K. Drozdov, B. Andrei Bernevig, and A. Yazdani, High-resolution studies of the Majorana atomic chain platform, *Nature Physics* **13**, 286 (2017).
- [39] M. Ruby, B. W. Heinrich, Y. Peng, F. von Oppen, and K. J. Franke, Exploring a proximity-coupled Co chain on Pb(110) as a possible Majorana platform, *Nano Letters* **17**, 4473 (2017).
- [40] L. Schneider, P. Beck, J. Neuhaus-Steinmetz, L. Rózsa, T. Posske, J. Wiebe, and R. Wiesendanger, Precursors of Majorana modes and their length-dependent energy oscillations probed at both ends of atomic Shiba chains, *Nature Nanotechnology* **17**, 384 (2022).
- [41] E. Liebhaber, L. M. Rütten, G. Reecht, J. F. Steiner, S. Rohlf, K. Rosnagel, F. von Oppen, and K. J. Franke, Quantum spins and hybridization in artificially-constructed chains of magnetic adatoms on a superconductor, *Nature Communications* **13**, 2160 (2022).
- [42] T. I. Tügel, V. Chua, and T. L. Hughes, Embedded topological insulators, *Physical Review B* **100**, 115126 (2019).
- [43] E. N. Economou, *Green's Functions in Quantum Physics*, Springer Series in Solid-State Sciences, Vol. 7 (Springer Berlin Heidelberg, Berlin, Heidelberg, 2006).
- [44] Z. Wang and S.-C. Zhang, Simplified topological invariants for interacting insulators, *Physical Review X* **2**, 031008 (2012).
- [45] Z. Wang and B. Yan, Topological Hamiltonian as an exact tool for topological invariants, *Journal of Physics: Condensed Matter* **25**, 155601 (2013).
- [46] V. Gurarie, Single-particle Green's functions and interacting topological insulators, *Physical Review B* **83**, 085426 (2011).
- [47] S. Tewari and J. D. Sau, Topological invariants for spin-orbit coupled superconductor nanowires, *Physical Review Letters* **109**, 150408 (2012).
- [48] C.-K. Chiu, J. C. Teo, A. P. Schnyder, and S. Ryu, Classification of topological quantum matter with symmetries, *Reviews of Modern Physics* **88**, 035005 (2016).
- [49] B. Braunecker, G. I. Japaridze, J. Klinovaja, and D. Loss, Spin-selective Peierls transition in interacting one-dimensional conductors with spin-orbit interaction, *Physical Review B* **82**, 045127 (2010).
- [50] B. Braunecker and P. Simon, Interplay between classical magnetic moments and superconductivity in quantum one-dimensional conductors: Toward a self-sustained topological Majorana phase, *Physical Review Letters* **111**, 147202 (2013).
- [51] Y. Kim, M. Cheng, B. Bauer, R. M. Lutchyn, and S. Das Sarma, Helical order in one-dimensional magnetic atom chains and possible emergence of Majorana bound states, *Physical Review B* **90**, 060401 (2014).
- [52] J. Klinovaja, P. Stano, A. Yazdani, and D. Loss, Topological superconductivity and Majorana fermions in RKKY systems, *Physical Review Letters* **111**, 186805 (2013).
- [53] M. M. Vazifeh and M. Franz, Self-organized topological state with Majorana fermions, *Physical Review Letters* **111**, 206802 (2013).
- [54] M. Schechter, M. S. Rudner, and K. Flensberg, Spin-lattice order in one-dimensional conductors: Beyond the RKKY effect, *Physical Review Letters* **114**, 247205 (2015).
- [55] M. Schechter, K. Flensberg, M. H. Christensen, B. M. Andersen, and J. Paaske, Self-organized topological su-

- perconductivity in a Yu-Shiba-Rusinov chain, *Physical Review B* **93**, 140503 (2016).
- [56] D. Varjas, T. Ö. Rosdahl, and A. R. Akhmerov, Qsymm: algorithmic symmetry finding and symmetric Hamiltonian generation, *New Journal of Physics* **20**, 093026 (2018).
- [57] T. L. Hughes, E. Prodan, and B. A. Bernevig, Inversion-symmetric topological insulators, *Physical Review B* **83**, 245132 (2011).
- [58] I. Peschel, Calculation of reduced density matrices from correlation functions, *Journal of Physics A: Mathematical and General* **36**, L205 (2003).
- [59] A. Alexandradinata, T. L. Hughes, and B. A. Bernevig, Trace index and spectral flow in the entanglement spectrum of topological insulators, *Physical Review B* **84**, 195103 (2011).
- [60] L. Fidkowski, Entanglement spectrum of topological insulators and superconductors, *Physical Review Letters* **104**, 130502 (2010).
- [61] S. Ryu and Y. Hatsugai, Entanglement entropy and the Berry phase in the solid state, *Physical Review B* **73**, 245115 (2006).
- [62] J. C. Budich and E. Ardonne, Equivalent topological invariants for one-dimensional Majorana wires in symmetry class D, *Physical Review B* **88**, 075419 (2013).